

***Sens-BERT*: Enabling Transferability and Re-calibration of Calibration Models for Low-cost Sensors under Reference Measurements Scarcity**

M V NARAYANA, Department of Electrical Engineering, IITM, India

KRANTHI KUMAR RACHAVARAPU, Department of Electrical Engineering, IITM, India

DEVENDRA JALIHAI, EE Department, IITM, India

SHIVA NAGENDRA S M, CE Department, IITM, India

Low-cost sensors (LCS) are becoming increasingly relevant for monitoring and understanding air quality at high spatial and temporal resolution. However, LCS measurements are noisy, which limits large-scale adaptability. Calibration is generally used to get good estimates of air quality measurements out from LCS. In order to do this, LCS sensors are typically co-located with reference stations for some duration. A calibration model is then developed to transfer the LCS sensor measurements to the reference station measurements. Existing works implement the calibration of LCS as an optimization problem in which a model is trained with the data obtained from real-time deployments; later, the trained model is employed to estimate the air quality measurements of that location. However, this approach is sensor-specific and location specific and needs frequent re-calibration. The re-calibration also needs massive data like initial calibration, which is a cumbersome process in practical scenarios.

To overcome these limitations, in this work, we propose *Sens-BERT*, a BERT-inspired learning approach to calibrate LCS, and it achieves the calibration in two phases: self-supervised pre-training and supervised fine-tuning. In the pre-training phase, we train *Sens-BERT* with only LCS data (without reference station observations) to learn the data distributional features and produce corresponding embeddings. We then use the *Sens-BERT* embeddings to learn a calibration model in the fine-tuning phase. Our proposed approach has many advantages over the previous works. Since the *Sens-BERT* learns the behavior of the LCS, it can be transferable to any sensor of the same sensing principle without explicitly training on that sensor. It requires only LCS measurements in pre-training to learn the characters of LCS, thus enabling calibration even with a tiny amount of paired data in fine-tuning. We have exhaustively tested our approach with the Community Air Sensor Network (CAIRSENSE) data set, an open repository for LCS. We show that the proposed method outperforms well-known calibration models such as single-variable linear regression, multiple-variable linear regression, and Random forest models.

Additional Key Words and Phrases: Low-cost sensors, Calibration, Representation Learning, BERT

1 INTRODUCTION

Air pollution is a significant environmental concern that affects human health and well-being. Monitoring air quality is crucial for understanding the levels of pollutants in the atmosphere and taking appropriate actions to mitigate their effects. While professional-grade air quality monitoring (AQM) systems are widely used, they can be expensive and limited in availability [1]. To address this issue, low-cost sensors (LCS) for AQM have emerged as a viable solution. LCS provide an affordable and accessible means of measuring various air pollutants, enabling individuals, communities, and organizations to monitor their local air quality actively [2–4]. These sensors utilize innovative technologies and compact designs to deliver real-time data on pollutant concentrations, enabling timely responses and informed decision-making. LCS can measure parameters such as particulate matter (*PM*), gases like carbon dioxide (CO_2), carbon monoxide (*CO*), nitrogen dioxide (NO_2), and volatile organic compounds (*VOCs*). They may also include temperature (*T*) and humidity (*Rh*) sensors to assess environmental conditions comprehensively.

Despite these advantages, the measurements produced by the LCS are susceptible to various error sources that can affect the accuracy, rendering the LCS less reliable than the reference grade instruments. Typical error sources include variations in temperature and relative humidity, cross-sensitivities (sensitive towards pollutants that existed other than the target parameters) and drift [5, 6]. Therefore, proper calibration is crucial to address these

issues, and by doing so, we can improve the accuracy of LCS measurements [7]. Calibration involves transforming the LCS measurements to align with reference station observations.

Applying correction factors to the sensor signal for the respective parameters influencing its response is a preliminary way to calibrate the LCS [8–11]. For instance, \mathcal{S} is an LCS signal, which corrects for the effect of temperature (T) and relative humidity (Rh) in the equation below.

$$\hat{\mathcal{S}} = \mathcal{S} + \alpha_1(T) + \alpha_2(Rh) \quad (1)$$

where $\alpha_1(\cdot)$ and $\alpha_2(\cdot)$ are the correction factors modelled by exposing the LCS to various T and Rh values in controlled environments. The correction factors are sensor specific and often derived based on a limited number of calibration points. As a result, they may not accurately account for variations in the sensor’s response across its entire operating range. At the same time, LCS may experience calibration drift over time due to environmental factors, sensor ageing, or changes in response characteristics which needs the frequent modelling of calibration factors, which is a cumbersome process in practice.

To overcome the limitations in the correction factors approach, a learning-based approach is proposed to calibrate the LCS [12–14]. In this approach, calibration of LCS is framed as an optimisation problem, where a calibration model (f_θ) is trained to minimise the mean square error (MSE) between the LCS measurements (\mathcal{X}_t) and reference station observations (\mathcal{Y}_t). Since the calibration models are trained with ambient conditions in real-time deployments, they can handle the error sources effectively, provided they are trained on a substantial amount of the data that covers all these variables. However, in the existing learning-based calibration works, the calibration model is sensor-specific and location-specific since their optimization is limited to a particular scenario, and they do not generalize the characteristics of the LCS measurements. Due to this, their calibration accuracy is limited, and transferring the calibration models trained on one sensor to other sensors further limits their effectiveness in calibrating the Low-cost sensors. At the same time, it needs frequent re-calibration to handle the calibration drift, which requires substantial co-location measurements of LCS and reference stations.

In summary, the existing learning-based works mainly focus on transforming the LCS measurements without learning their distributional characteristics, such as temporal and environmental dependencies. It is essential to learn the distributional information of measurements to generalize the calibration model to the LCS and to improve the calibration accuracy with limited paired data. To address these limitations, we propose *Sens-BERT*, a BERT-based (Bidirectional Encoder Representations from Transformers) [15] approach to calibrate the Low-cost sensors and it achieves the calibration in two steps: pre-training and fine-tuning. The pre-training step is self-supervised, where a BERT-based model, *Sens-BERT*, is trained only on LCS measurements without using the reference station observations, and this pre-training enables *Sens-BERT* to learn the characteristics of LCS measurement. Therefore, the pre-trained *Sens-BERT* can produce the embeddings corresponding to the LCS measurements, which are then used in the fine-tuning step, where a calibration model can be trained with limited paired data. At the same time, the pre-trained *Sens-BERT* can be utilized in the re-calibration, and it can be transferred to other sensors of the same sensing principle that needs to be calibrated since it already learned the data characteristics.

To the best of our knowledge, this is the first work that implements a BERT-based approach to calibrate the LCS, and our contributions are as follows,

- We implement a BERT-based deep learning architecture, *Sens-BERT*, to learn the characteristics of LCS measurements, which enables calibration and re-calibration with limited paired data.
- We empirically validate the transferability of *Sens-BERT* to other sensors without explicitly pre-training it on those sensors.
- We show that the proposed approach outperforms the existing optimization-based calibration works for different sensors in the CAIRSENSE data set [16], an open repository for the LCS.

2 RELATED WORK

Calibration approaches for low-cost sensors (LCS) have been an active area of research, and several works have been disseminated to enhance the accuracy of LCS through calibration. This section summarises the existing works on the calibration of LCS.

Laboratory and field studies. Numerous laboratory and field investigations have been undertaken to gather data from LCS deployed in diverse environments [17–20]. This data collection enables examining sensor responses across different conditions and provides valuable inputs for developing calibration techniques. Concurrently, comparing LCS measurements with those obtained from established air quality monitoring stations facilitates the validation of LCS performance.

Correction factors approach. The data collected in both field and laboratory settings enables the development of correction factors for sensor response, effectively addressing biases in the sensor response. Carl et al. [21] and Barkjohn et al. [22] applied hygroscopic growth factor correction to PM sensor response in order to correct the effect of relative humidity on PM sensors. Similarly, the gas sensors also corrected for meteorological parameters to improve accuracy [8, 10, 23].

Machine learning-based calibration. Machine learning algorithms have been employed to calibrate LCS. The algorithm learns the relationship between the sensor responses and the actual pollutant concentrations by training the algorithm on data collected from LCS and corresponding reference instruments. This enables the algorithm to make more accurate predictions and calibrate the sensor readings. These models include single-variable linear regression[24–27], multiple-variable linear regression[24, 28, 29], K-nearest neighbours[28], random forest[13, 30–32], artificial neural networks[12, 14, 31, 33, 34], support vector machine [35, 36], Extreme Gradient Boosting[37], generalised additive model [38]. In addition, a few works explored hybrid models obtained by combining two or more ML to calibrate the LCS [39–41]. For instance, Hagan et al. [40] and Lin et al. [39] combined the regression model with the k-nearest neighbours and random forest, respectively, to improve the calibration accuracy compared to the stand-alone models. A similar approach that combines regression models with ANN was implemented by Cordero et al. [42]; instead of connecting the models, Ferrer-Cid et al. used multi-sensor data fusion techniques to calibrate the LCS [43].

In the existing machine-learning-based calibration works, the calibration of low-cost sensors is not transferable to other sensors since they learn from sensor-specific data alone instead of the general characteristics of LCS. Therefore, it requires a substantial amount of real-time deployment data for every recalibration, which is necessary to overcome the calibration drift problem. In contrast, *Sens-BERT*, proposed in this work, first learns the data representation from low-cost sensors measurements alone, which enables the transfer of the *Sens-BERT* to other sensors. At the same time, it can be calibrated with limited data for real-time deployments.

3 APPROACH

This work aims to learn the representations of low-cost sensors (LCS) measurements with BERT architecture and needs to calibrate the LCS with limited paired data in real-time deployments. To accomplish the task, we first frame the calibration of LCS as a BERT-based deep learning model (*Sens-BERT*) optimization (Sec 3.1). Then we cover the characteristics of LCS measurements (Sec 3.2), which helps to tailor the input to the *Sens-BERT*. Finally, we describe the architecture of *Sens-BERT* in Sec 3.3.

3.1 Problem formulation: implementation of calibration of LCS as a BERT-based deep learning model

In low-cost sensor calibration, the goal is to transform the LCS measurements to reference station observations. Specifically, given a set of measurements of LCS and reference station observations, $\{\mathcal{X}_t, \mathcal{Y}_t\}_{t=1}^T$, our objective is to learn a regression model that transforms $\mathcal{X}_t \in \mathbb{R}^{N \times K}$ to $\mathcal{Y}_t^{N \times 1}$. Here, \mathcal{X}_t consist N of measurements from each K low-cost sensors such as temperature (T), relative humidity (Rh), pollutant of interest like $PM_{2.5}$, CO_2

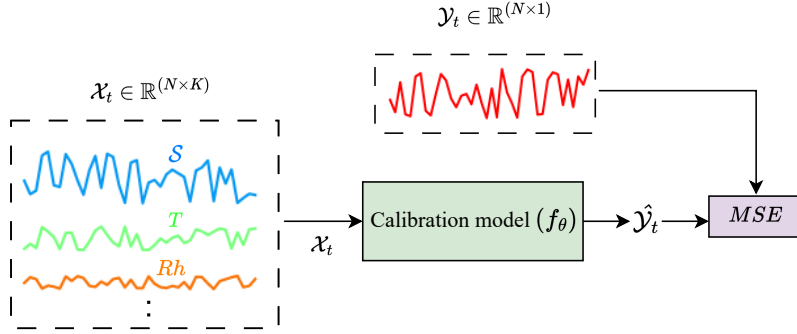


Fig. 1. Calibration of LCS as an optimization problem in the existing works

etc., and \mathcal{Y}_t consists corresponding reference station observations. Traditionally, this problem is approached as a learning-based optimization problem, as shown in Fig. 1, where the parameters (θ) of a calibration model (f_θ) are optimized such that it can transform \mathcal{X}_t to \mathcal{Y}_t , as shown in equations (2) and (3).

$$\hat{\mathcal{Y}}_t = f_\theta(\mathcal{X}_t) \quad \forall t \quad (2)$$

$$\theta^* = \arg \min_{\theta} \frac{1}{N} \sum_{t=1}^N \text{MSE}(\hat{\mathcal{Y}}_t, \mathcal{Y}_t) \quad (3)$$

However, the measurements in \mathcal{X}_t show temporal dependency, which means the current observations are greatly influenced by previous measurements [44], and these temporal dependencies cannot be tackled by the traditional approaches. Therefore, it needs to be hypothesised that the calibration model (f_θ) can learn the temporal dependencies and other distributional information of \mathcal{X}_t to improve calibration accuracy, as shown in equation (4).

$$\hat{\mathcal{Y}}_t = f_\theta(\mathcal{X}_{t-M}, \mathcal{X}_{t-M-1}, \dots, \mathcal{X}_t) \quad \forall t \quad (4)$$

Where M is the temporal context slice which is the experimental hyperparameter. Since the calibration model f_θ in equation (4) focuses only on transforming \mathcal{X}_t to \mathcal{Y}_t without learning the temporal dependencies and distributional information, it needs to alter the f_θ such that it can learn the characteristics of the measurements first and then it can transform the LCS measurements to reference station observations.

We propose a two-step calibration framework shown in Fig. 2 to implement such a calibration process. In the proposed approach, we first focus on learning the temporal dependencies and other distributional information of \mathcal{X}_t in the self-supervised pre-training step using a BERT-based deep learning architecture, *Sens-BERT*. The *Sens-BERT* shown in Fig. 2 inherits an encoder and decoder to learn the characteristics of LCS measurements. To force the *Sens-BERT* to learn the characteristics of LCS measurements, we mask sequences of samples in \mathcal{X}_t using the span masking technique [45] with probability P and then operated a sliding window of length M with an overlapping length of O_l between two successive windows such that it can feed the *Sens-BERT* with temporal context. Let $\mathcal{X} \in \mathbb{R}^{M \times K}$ is a sample obtained by operating sliding window on \mathcal{X}_t at time t , then the encoder transforms the measurements in \mathcal{X} , including masked samples, into embeddings (\mathcal{E}), and the decoder re-transforms \mathcal{E} to $\hat{\mathcal{X}}$, which is the estimated \mathcal{X} . Therefore, in the pre-training phase, *Sens-BERT* transforms \mathcal{X} to \mathcal{E} and then to $\hat{\mathcal{X}}$ as shown in equations (5) and (6) and learns the characteristics of \mathcal{X}_t while doing these transformations, by minimizing the loss in equation (7), that is, the *MSE* between \mathcal{X} and $\hat{\mathcal{X}}$.

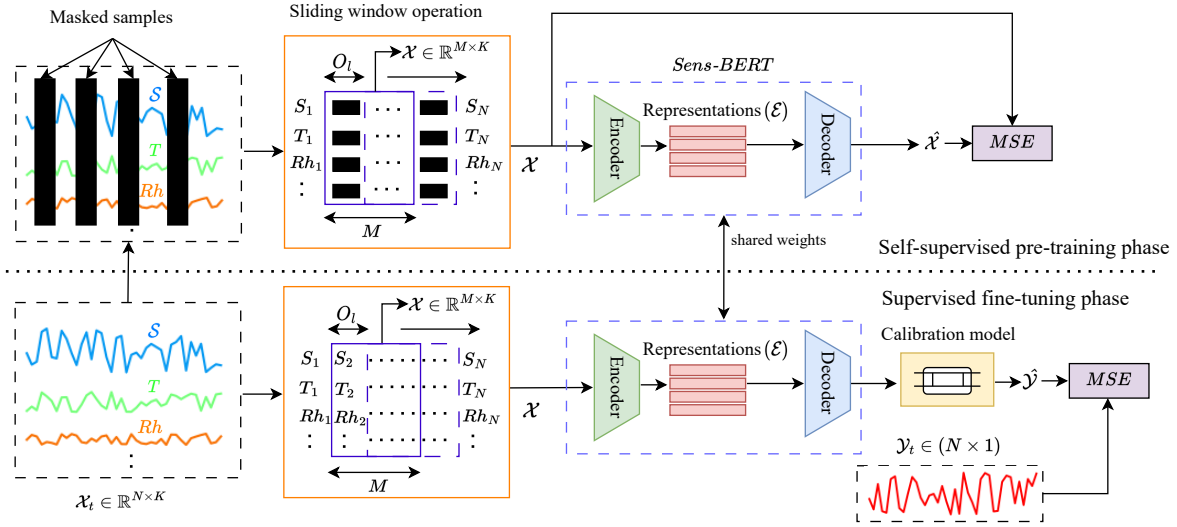


Fig. 2. Calibration of Low-cost sensors with Sens-BERT

$$\mathcal{E} = f_{enc}(\mathcal{X}); \quad \mathcal{X} \in \mathbb{R}^{M \times K} \sim \{\mathcal{X}_t\}_{t=1}^T \quad \forall t \quad (5)$$

$$\hat{\mathcal{X}} = f_{dec}(\mathcal{E}) \quad (6)$$

$$\text{loss}_{\text{pre-train}} = \frac{1}{N} \sum_{i=1}^N \text{MSE}(\mathcal{X}, \hat{\mathcal{X}}) \quad (7)$$

Once Sens-BERT is trained in pre-training, it can be used in the second step, which is a fine-tuning phase, where a calibration model (f_{θ}) is trained with generated embedding against the reference station observations \mathcal{Y}_t , as shown in the below equations.

$$\hat{\mathcal{X}} = \text{Sens-BERT}(\mathcal{X}) \quad \forall t \quad (8)$$

$$\hat{\mathcal{Y}}_t = f_{\theta}(\hat{\mathcal{X}}) \quad (9)$$

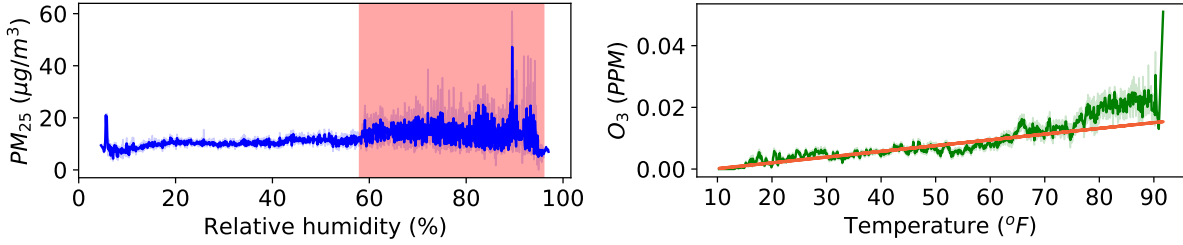
$$\text{loss}_{\text{fine-tune}} = \frac{1}{N} \sum_{t=1}^N \text{MSE}(\hat{\mathcal{Y}}_t - \mathcal{Y}_t) \quad (10)$$

Since our approach learns the temporal dependencies and other distributional information of the LCS measurements, it can calibrate the LCS effectively with limited paired data. At the same time, the pre-trained Sens-BERT can be transferred to other sensors, which need to be calibrated.

3.2 Characteristics of LCS data

Generally, low-cost sensors predominant in AQM are divided into particle sensors that work on the light scattering principle and gas sensors that work on metal oxide or electro-chemical principle. Particle sensors are greatly influenced by relative humidity (Rh) due to the hygroscopic properties of the particulate matter (PM) [41]. At higher relative humidity, tiny particles floating around (aerosols) tend to stick together more because of the water

vapour, which significantly changes the amount of scattered light, thus changing the response of the sensors. To illustrate the effect of relative humidity on particle sensors, we plotted sample data of AirAssure, an LCS that works on the light scattering principle from the CAIRSESE data set [16] in Fig. 3(a). The graph is plotted between the PM_{25} (PM of size less than $0.25 \mu m$) on the y-axis and Rh on the x-axis. From Fig. 3(a), it can be observed that the PM_{25} values have evident fluctuations for higher Rh , which is highlighted in red shade.



(a) Relative humidity effect on particle sensors

(b) Temperature effect on metal oxide gas sensors)

Fig. 3. Effect of temperature and relative humidity on the response of low-cost sensors. The plots are drawn with the data from the CAIRSENSE data set [16].

Temperature (T) and relative humidity (Rh) are the prime environmental factors influencing the accuracy of gas sensors. These factors influence the resistance of the heating element under the metal oxide surface in metal-oxide sensors; thus, changing its sensitivity causes inaccurate measurements [8, 46]. Fig. 3(b), plotted between the temperature and response of Aeroqual, a metal oxide sensor measures O_3 , shows the apparent drift (drift in trend line) in the response with increase in temperature. In the case of electrochemical sensors, temperature changes the rate of the chemical reaction and moisture content depletes the sensors' electrodes, thus changing the response of the sensors [11]. Further, they suffer from cross-sensitive issues, which means they are also sensitive to other gasses in the atmosphere [47, 48].

Based on the above observations, we select the variables that need to be considered in the calibration implementation, discussed in Sec. 4.

3.3 Sens-BERT

Sens-BERT, shown in Fig. 2, is implemented on BERT architecture, consisting of an encoder and a decoder. Encoders transform the given sequences (\mathcal{X}) into embeddings ($\mathcal{E} \in \mathbb{R}^{H_{dim} \times M}$), and the decoder re-transforms the embeddings into sequences, as represented in the below equations.

$$\begin{array}{l}
 \textbf{Sens-BERT} \\
 \mathcal{X} \sim \{\mathcal{X}_t\}_{t=1}^T \quad \forall t \\
 \mathcal{E} = f_{enc}(\mathcal{X}) \\
 \hat{\mathcal{X}} = f_{dec}(\mathcal{E})
 \end{array}$$

While doing these transformations, it learns the characteristics of low-cost sensor measurements by minimizing the loss equation in (7). The *Sens-BERT* that learned the characteristics of LCS can be utilised to calibrate the LCS with limited paired data. At the same time, it can be transferable to other sensors that need a fresh calibration without explicitly training the *Sens-BERT* on those sensors. Calibration of LCS with *Sens-BERT* can be achieved in two steps -

- (1) *Self-supervised pre-training* to learn good representations using low-cost sensor measurements alone.
- (2) *Supervised fine-tuning* to learn the final calibration model.

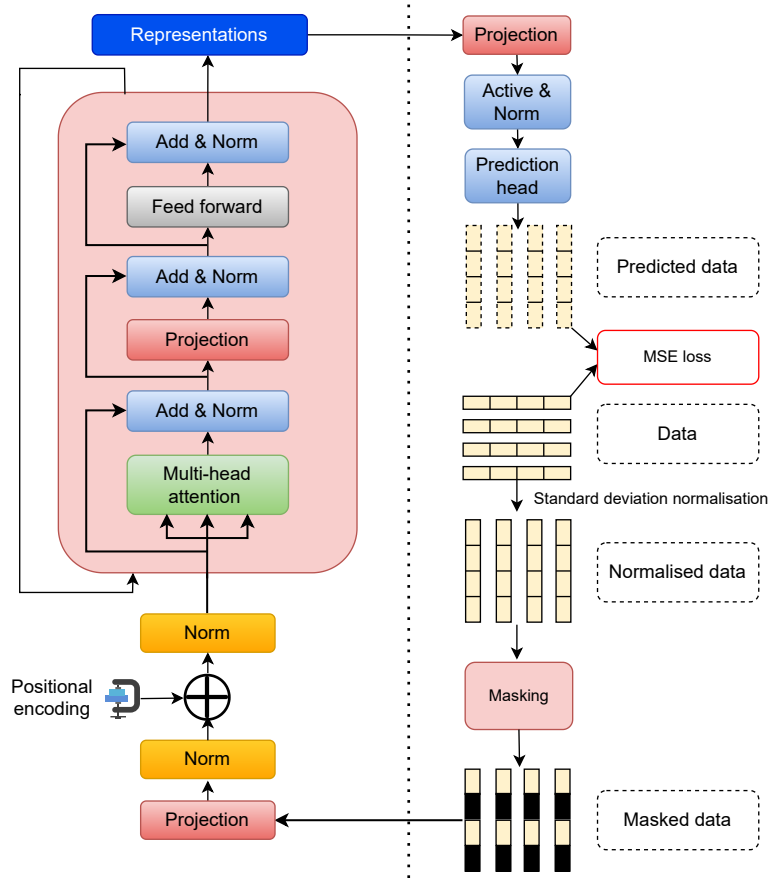


Fig. 4. Self-supervised pre-training phase of Sens-BERT with transformer architecture

3.3.1 Self-supervised pre-training phase. The objective of the pre-training phase is to learn the representations of LCS measurements (\mathcal{X}_t) with *Sens-BERT*, and the sequence of steps involved in the pre-training phase are illustrated in Fig 4. To force *Sens-BERT* to learn the representations of \mathcal{X}_t , we first mask the sequence of samples in \mathcal{X}_t with probability P by using the span masking technique [45]. Next, we operated a sliding window of size M on \mathcal{X}_t as shown in equation (11), to slice M samples from \mathcal{X}_t at every time t . Where M is the temporal context slice, an experimental parameter, K is the number of variables (parameters considered for calibration) in \mathcal{X}_t and N is the number of samples. The sliding window operation enables to pass temporal context to the *Sens-BERT*, so it can learn the temporal dependencies in the measurements.

$$\mathcal{X} \in \mathbb{R}^{M \times K} \sim \{\mathcal{X}_t\}_{t=1}^T ; \mathcal{X}_t \in \mathbb{R}^{N \times K}, \mathcal{X} = \{\mathcal{X}_{t-M}, \mathcal{X}_{t-M-1} \dots \mathcal{X}_t\} \forall t \quad (11)$$

Then we apply projection ($\mathbf{Proj}(\cdot)$) operation to the input sequences in \mathcal{X} . Since the number of features or variables (K) in \mathcal{X} is tiny to feed to the BERT architecture [49], that is, the encoder and decoders of *Sens-BERT*, it

needs to project the measurements in \mathcal{X} to higher dimensional space, and we implemented this by using a linear layer shown in equation (12).

$$D = \mathbf{Proj}(\mathcal{X}) = \mathbf{W}^T \mathcal{X} \quad (12)$$

Where \mathbf{W} is a weight matrix of size $H_{dim} \times K$ and H_{dim} is the hidden dimension size, the dimension expansion parameter of the neural networks. Once the values in \mathcal{X} transform to higher dimensional space D , the vectors in D need to be normalized to train the transformer-based architectures effectively [50]. We applied the layer normalization technique proposed by Jimmy et al. [50] shown in equation (13) in our experimentation to normalize the values in D .

$$D'_{ji} = \text{LayerNorm}(D) = \frac{D_{ji} - \mu_j}{\sqrt{(\sigma_j^2 + \epsilon)}} \cdot \gamma + \beta \quad (13)$$

Where μ_j and σ_j are the mean and standard deviation of j^{th} column of D , i is the row number and ϵ is a small number to eliminate the occurrence of infinite for zero value of σ . γ and β are the learning hyperparameters that help neural networks learn the dynamical normalization of features. Note that where ever the projection and normalization come in pre-training, it does the same in equations (12) and (13).

Once the values in D are normalized, it is added with the positional encoding with the help of a positional embedding function $PE(\cdot)$ [49], which maps the column (j) index of D to a vector of length H_{dim} . Positional encoding helps to preserve the order of information that can be utilized at the decoder. Then, the data is passed through second-layer normalization, and the output after second-layer normalization, that is, the hidden features, are expressed as follows:

$$\mathcal{H}_{.j} = \text{LayerNorm}(D'_{.j} + PE(j)) \quad (14)$$

Then, the attention-entic block shown in Fig. 4 (big pink rectangular box) takes H as input and repeats for R_{num} of times before producing the final representations \mathcal{E} . It performs the two primary operations, Multi-head attention (**Multi-Attn**(\cdot)) and feed-forward (**FeedFrd**(\cdot)) operations, with projection and layer normalization after every operation. The **Multi-Attn**(\cdot) is the self-attention layer of the transformer architecture [49] with multiple attention heads. Here, we employ the scaled dot-product attention mechanism to learn the latent interaction within the embeddings, which can be considered as transforming three sets of LCS measurements, i.e., Query, Key, and Value representation. Here, the attention score is generated from Query and Key. Then, the Value vector is weighted according to the attention score to generate the final embedding. The **FeedFrd**(\cdot) operation enables the element-wise non-linearity transformation of incoming embeddings. We implemented the feed-forward operation using two fully connected layers coupled with a Gaussian Error Linear Unit (GELU) [51] activation function.

$$\{\mathcal{H} = \text{LayerNorm}(\mathbf{FeedForward}(\text{LayerNorm}(\mathbf{Proj}(\text{LayerNorm}(\mathbf{Multi-Attn}(\mathcal{H}))))))\}^{R_{num}} = \mathcal{E} \in \mathbb{R}^{H_{dim} \times M} \quad (15)$$

Finally, the embeddings produced by the attention-entic block are passed to the decoder to reconstruct the masked samples. The decoder implementation involves a projection layer, an activated and normalization layer and a prediction head. At first, the projection layer projects the embeddings, \mathcal{E} , into D . Then the prediction layer (**Pred**(\cdot)), followed by $\text{LayerNorm}(\cdot)$ operation, reconstructs $\hat{\mathcal{X}}$ from the D .

$$D = \text{Proj}(\text{GELU}(\mathcal{E})) \quad (16)$$

$$\hat{\mathcal{X}} = \text{LayerNorm}(\mathbf{Pred}(D)) \quad (17)$$

Putting all the operations together, the *self-supervised pre-training phase* transforms \mathcal{X} into \mathcal{E} then to $\hat{\mathcal{X}}$ and makes *Sens-BERT* learn the characteristics of low-cost sensor measurements while doing these transformations by minimizing the loss in the below equation.

$$\text{loss}_{\text{pre-train}} = \frac{1}{N} \sum_{i=1}^N \text{MSE}(\mathcal{X}, \hat{\mathcal{X}})$$

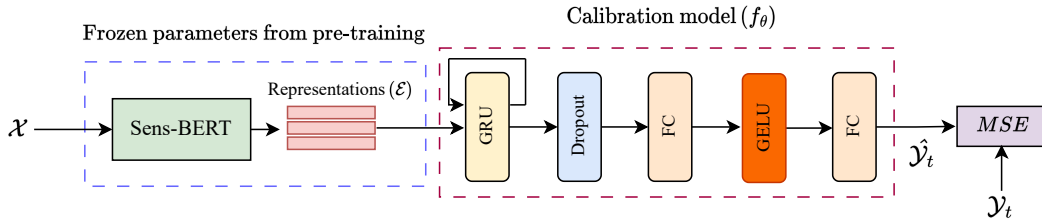


Fig. 5. Supervised fine-tuning phase of calibration model with trained *Sens-BERT*

3.3.2 Supervised fine-tuning phase. The trained *Sens-BERT* with frozen parameters can be utilized in the supervised fine-tuning phase, where a calibration-specific model can be trained with the limited paired data. The calibration-specific model is of user interest, and we implemented this by stacking three Gated Recurrent Unit (GRU) layers [52], one drop-out layer and two fully connected layers one on another, as shown in Fig. 5. Specifically, for given observations $\{\mathcal{X}, \mathcal{Y}_t\}$, where $\mathcal{X} \in \mathbf{R}^{M \times K} \sim \{\mathcal{X}_t\}_{t=1}^T$ at time t , is the low-cost sensor measurements from K sensors over M , $\mathcal{Y}_t \in \mathbf{R}$ is the reference station measurement, we first extract the embeddings using the pre-trained *sens-bert* encoder as,

$$\mathcal{E}_t = f_{enc}(\mathcal{X}_t) \in \mathbf{R}^{M \times d}, \quad (18)$$

where d is the embedding dimension. This embedding is then fed as input to the calibration model (f_θ) to predict the corrected sensor measurement $\hat{\mathcal{Y}}_t$ as,

$$\hat{\mathcal{Y}}_t = f_\theta(\mathcal{E}_t) = \text{FC}(\text{Dropout}(\text{GRU}(\mathcal{E}_t))). \quad (19)$$

Finally, the calibration-specific model is trained by minimizing the loss in equation (20), which can be used to obtain accurate pollution values from LCS.

$$\text{loss}_{\text{fine-tune}} = \frac{1}{N} \sum_{i=1}^N \text{MSE}(\mathcal{Y}_t, \hat{\mathcal{Y}}_t). \quad (20)$$

Therefore, *Sens-BERT* learns the characteristics of LCS measurements in the pre-training phase, which can be used to train a calibration model with limited paired data in the fine-tuning phase. Further, the trained *Sens-BERT* can be transferred to other sensors needing fresh calibration. The implementation details on the real-time data set are presented in Sec. 4.2, and the corresponding results are available in Sec. 4.3

4 EXPERIMENTS

4.1 Data sets

We evaluate our approach on Community Air Sensor Network (CAIRSENSE) data set, an open repository developed by Feinberg et al. [16] for low-cost sensors, and it is available at the US environmental protection (USEPA) data website [53]. The data set contains measurements from various low-cost sensors and the time corresponding temperature, relative humidity and reference saturation observations. The measurements are taken from the Colorado state at a one-minute resolution.

Details of the low-cost sensors considered from the CAIRSENSE data set are as follows,

- Shinyei - measures PM - works on light scattering principle
- SpecK - measures PM - work on light scattering principle
- OPCPMF - measures PM - works on light scattering principle
- TZOA - measures PM - work on light scattering principle
- AirAssure - measures PM - work on light scattering principle

4.2 Implementation details

As discussed in Sec. 3.1, calibration models aim to transform the raw sensor signal (S_t) to the corresponding reference station observations (\mathcal{Y}_t). Though it seems like handling a single variable (S_t) transformation, in practice, it needs to be handled more than one variable since the LCS performance is severely affected by other covariates discussed in Sec 3.2. Therefore, we framed the data set (\mathcal{X}_t) by including all the variables ($v_K; K = \{1, 2, \dots\}$) that affect the performance of the selected sensor as;

$$\mathcal{X}_t = [v_1 \quad v_2 \quad \dots, v_K]_{N \times K}$$

Where K is the number of variables, N is the number of samples and $v_k \in \mathbf{R}^{N \times 1}$ is the columns vector of measurements from K^{th} variable. In our experiments in Sec. 4.3, we consider output from the LCS (S), temperature (T) and relative humidity Rh as the variables in \mathcal{X}_t . $\mathcal{Y}_t \in \mathbf{R}^{N \times 1}$ are the time corresponding reference station observations to that of \mathcal{X}_t . Point to be noted that the K value depends on the sensor that needs to be calibrated and influencing factors in the sensor deployment site.

Elimination of outliers: We apply threshold-based filtering to discard the outlier samples. Since the air pollutants follow skewed distributions [32], we used the Inter-Quartile Range ($IQR = Q3 - Q1$) proximity rule to detect the outliers; that is, the data points that fall below $Q1 - 1.5 \times IQR$ or above $Q3 + 1.5 \times IQR$ are outliers, where $Q1$ and $Q3$ are the 25th and 75th percentile of the data, respectively.

Creation of overlapping sequences: The measurements in \mathcal{X}_t show temporal dependency, which means the current observations are greatly influenced by previous measurements [44]. To feed the temporal context to the *Sens-BERT*, we operated a sliding wind of length (M) 128 with overlapping (O_l) of $M - 1$ samples between two successive windows on \mathcal{X}_t . That means at time t ; we slice 128 samples in \mathcal{X}_t from t to $t - M$ to train *Sens-BERT* and we iterate this sliding window till the end of samples in \mathcal{X}_t . Here, M and O_l are the experimental hyperparameters.

Masking of samples: To ensure *Sens-BERT* learns characteristics of \mathcal{X}_t in pre-training, we have masked sequence of samples in \mathcal{X}_t using span masking technique [45] with probability (P) of 0.2. The length of subsequent samples (S_t) to mask and P are the experimental parameters.

Training and testing: We divide the data in $\{\mathcal{X}_t, \mathcal{Y}_t\}$ into training data ($\{\mathcal{X}_t^{train}, \mathcal{Y}_t^{train}\}$) and testing data ($\{\mathcal{X}_t^{test}, \mathcal{Y}_t^{test}\}$) in 0.9 and 0.1 ratios, respectively. We then pre-train the *Sens-BERT* with \mathcal{X}_t^{train} , fine-tune the calibration model (f_θ) and other reference models such as regression and RF models with the paired train data, and test with the testing data. We use Adam optimizer to store and update the parameters while training and testing [54].

4.3 Evaluations

In order to check the adaptability of *Sens-BERT* to calibrate the LCS, we have performed the following three evaluations, which show that it outperforms the existing models and solves the transferability and re-calibration of calibration models for low-cost sensors under reference measurements scarcity.

- (1) *Evaluation of Sens-BERT in the calibration of LCS* - to check whether *Sens-BERT* calibrates the LCS or not
- (2) *Evaluation of Sens-BERT under availability of limited paired data* – to verify the effectiveness of *Sens-BERT* under reference measurement scarcity
- (3) *Evaluation of Sens-BERT transferability to other sensors* – to find the pre-trained *Sens-BERT* on some sensor can transfer to other sensors

Table 1. Evaluation of *Sens-BERT* approach for different sensors in the CAIRSENSE data set. * indicates the model that outperforms. The relative improvement with *Sens-BERT* compared to the best model (RF), is shown is %.

Sensor	Model	R ² ↑	RMSE ↓
Shinyei	MLR	0.66	0.58
	RF	0.8	0.44
	<i>Sens-BERT</i> *	0.9 (12.5%)	0.23 (47.7)
AirAssure	MLR	0.63	0.61
	RF	0.75	0.5
	<i>Sens-BERT</i> *	0.86 (17.0 %)	0.3 (40%)
Speck	MLR	0.32	0.82
	RF	0.65	0.58
	<i>Sens-BERT</i> *	0.83 (27.6 %)	0.32 (44.8 %)
TZOA	MLR	0.4	0.75
	RF	0.75	0.49
	<i>Sens-BERT</i> *	0.86 (14.6 %)	0.29 (40.8 %)
OPCPMF	MLR	0.26	0.85
	RF	0.56	0.66
	<i>Sens-BERT</i> *	0.81 (44.4 %)	0.31 (53.3 %)

4.3.1 *Evaluation of Sens-BERT in the calibration of LCS.* Here, we first pre-train the *Sens-BERT* with X_t^{train} by following the procedure discussed in Sec. 3.3.1. Then we fine-tune the calibration model, f_θ , an LSTM-based model with X_t^{train}, Y_t^{train} by utilizing the embeddings produced by the the pre-trained *Sens-BERT*. Since the regression and RF models do not accept a bunch of samples ($X \in \mathbf{R}^{M \times K} \sim \{X_t\} \forall t$) at a time, we have flattened the sequence of samples in X for all the variables into a single array and passed them to the regression and RF models. For example, if the input consists of M samples with K variables, the flattened array consists of $M \times K$ values and is passed as a single sample to the regression and RF models. This flattening helps train the regression and RF models on the same data used for training the *Sens-BERT* and ensures fair performance comparisons. Once the training is finished, all models are tested with test data. The results of this experiment are presented in table 1, and the outperforming models are indicated with *.

Table 1 shows that *Sens-BERT* outperforms the MLR and RF models for all the sensors. There is a maximum improvement of 44.4% in R^2 and 53.3 % in $RMSE$ for the OPCPMF Sensor. At a minimum, there is a 12.5%

improvement in R^2 for Shinyei and a 40% improvement in $RMSE$ for AirAssure sensors. Therefore, *Sens-BERT* can be adopted for calibrating low-cost air quality sensors.

4.3.2 Evaluation of *Sens-BERT* under availability of limited paired data. The initial assumption of this experiment is that there is a scarcity of reference station observations (\mathcal{Y}_t). In contrast to the experiment in Sec. 4.3.1, Let's assume only a few measurements in \mathcal{X}_t^{train} has corresponding reference station observations in \mathcal{Y}_t^{train} . Then it is not possible to train the MLR and RF models on entire train data since they need paired data. However, *Sens-BERT* has the advantage of learning the characteristics of \mathcal{X}_t without having \mathcal{Y}_t observations. To implement the limited paired data experiments, we assume that only P % of samples in \mathcal{X}_t^{train} have corresponding reference station observations. We then train the calibration models with that P % data and test with the testing data. We repeat this by considering other P % samples in \mathcal{X}_t^{train} until it covers complete data of \mathcal{X}_t^{train} as shown in Fig. 6. Finally, we average the R^2 and $RMSE$ values obtained in testing for all the sets, and we repeat this experiment by increasing the P value, such that it equals 100%, represents the experiment in Sec 4.3.1. This procedure helps test models' calibration efficiency with limited paired data since we pass only limited paired data. Yet, we make models to expose a complete range of values.

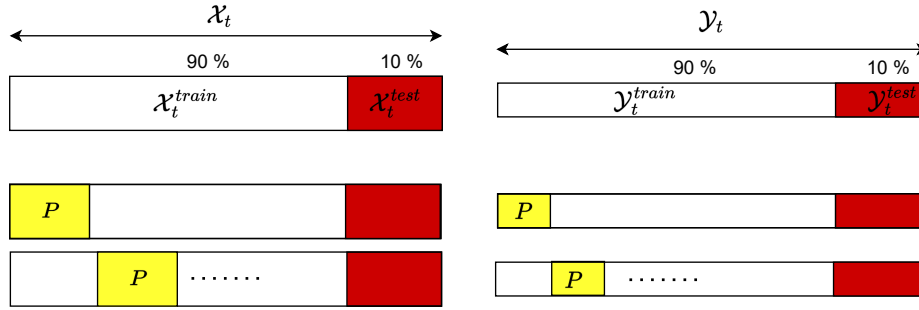
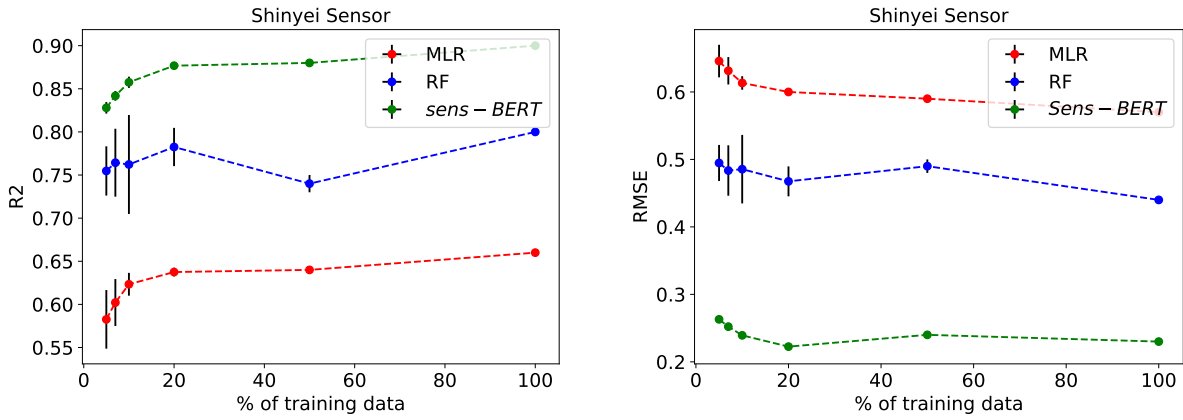


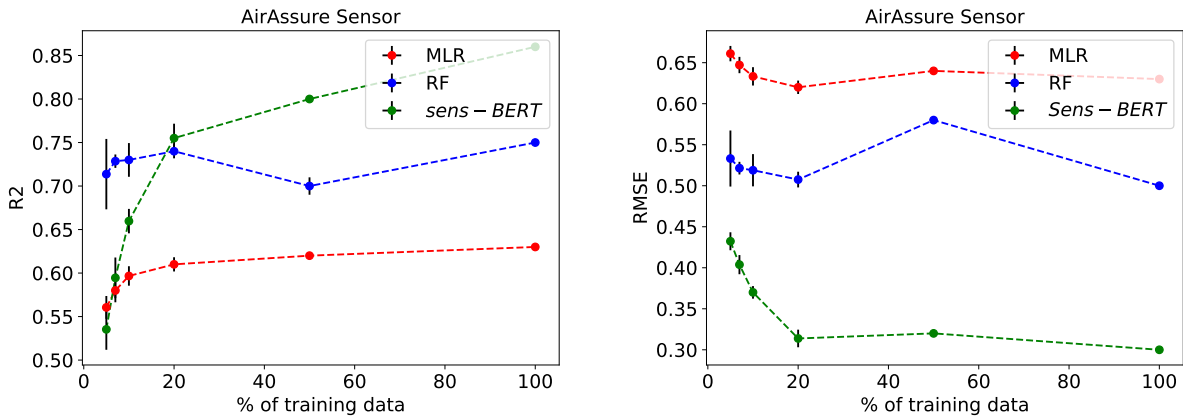
Fig. 6. Splitting of training data into chunks to test the calibration models under limited paired data

We expect the calibration accuracy of MLR and RF models increases as the P increases since these models can learn better with more paired data. In the case of calibration with *Sens-BERT*, we expect that it maintains the calibration accuracy even the P values decrease since it learns the characteristics of \mathcal{X}_t in pre-training and does not require more paired data to calibrate LCS. However, a too-low P value may also influence the calibration performance of *Sens-BERT* since a neural network architecture needs minimum data. We tested Shinyei and AirAssure sensors in this experiment, and the mean R^2 and $RMSE$ values with one standard deviation are presented in Fig. 7. Fig. 7 shows that For Shinyei Sensors, the *Sens-BERT* based calibration outperforms the MLR and RF models. However, in the case of AirAssure sensors, *Sens-BERT* require at least 20 % of the train data to fine-tune the LSTM-based calibration model (f_θ). After that, it outperforms both the MLR and RF models. Due to computational constraints, we have experimented on two sensors, and we expect the *Sens-BERT* based calibration can work for other sensors under reference measurement scarcity.

4.3.3 Evaluation of transferability of *Sens-BERT* to other sensors. In this experiment, we first adopt the pre-trained models mentioned in Sec. 4.3.1. Then we fine-tune the pre-trained models with other sensors' train data and test with the test data. For example, if a model is pre-trained on the data of sensor $K1$, then it is fine-tuned with the train data of sensor $K2$ and tested with the testing data of the $K2$. This process helps check the transferability of the models trained on one sensor to another. The experimental results for training on the AirAssure sensor and testing on Shinyei sensors are presented in Table 2.



(a) R^2 and $RMSE$ for Shinyei sensor



(b) R^2 and $RMSE$ for AirAssure sensor

Fig. 7. Mean R^2 and $RMSE$ values of different calibration models with one standard deviation with varying amounts of training data

5 CONCLUSIONS AND FUTURE SCOPE

This work proposes *Sens-BERT*, a BERT-based deep learning calibration approach for calibrating low-cost sensors for air quality monitoring. *Sens-BERT* outperforms the regression and random forest machine learning algorithms, which are extensively used in low-cost sensor calibration. We empirically validated the calibration performance of *Sens-BERT* on different low-cost sensors from the CAIRSENSE data set, available on US Environmental Protection Agency (USEPA) data website. *Sens-BERT* enables the re-calibration, the frequent calibration after sensor deployment to overcome the calibration drift, with limited paired data. We tested the performance of *Sens-BERT* under limited paired data by varying Further, *Sens-BERT* trained on one sensor can be transferred to other sensors. However, we tested the transferability on sensors working on the same sensing principle, that means if *Sens-BERT* is trained on a sensor works on an optical principle, we transferred the trained *Sens-BERT* to

Table 2. Testing transferability of calibration models

(a) Trained on AirAssure				(b) Trained on Speck			
Model	tested on	$R^2 \uparrow$	$RMSE \downarrow$	Model	tested on	$R^2 \uparrow$	$RMSE \downarrow$
MLR	Speck	0.04	1.02	MLR	Speck	0.32	0.82
	TZOA	0.13	0.9		TZOA	-2.29	1.75
	Shinyei	0.48	0.72		Shinyei	-0.19	1.09
	AirAssure	0.66	0.58		AirAssure	0.27	0.85
RF	Speck	0.02	0.99	RF	Speck	0.65	0.58
	TZOA	0.53	0.66		TZOA	0.01	0.96
	Shinyei	0.65	0.59		Shinyei	0.52	0.69
	AirAssure	0.75	0.5		AirAssure	0.19	0.9
Sens-BERT	Speck	0.7	0.36	Sens-BERT	Speck	0.83	0.29
	TZOA	0.73	0.32		TZOA	0.73	0.35
	Shinyei	0.8	0.34		Shinyei	0.78	0.34
	AirAssure	0.86	0.3		AirAssure	0.7	0.39

other sensors that also work on optical principle. Checking transferability between sensors works on different sensing principles is our future work.

In general performance of the BERT-based model improves if it learns a good representation of data. On that note, we expect that *Sens-BERT* trained on a substantial amount of low-cost sensor measurements curated from various data sets and websites makes it more powerful. However, it needs more computational capacity, which is a constraint for us now.

REFERENCES

- [1] Aakash C. Rai, Prashant Kumar, Francesco Pilla, Andreas N. Skouloudis, Silvana Di Sabatino, Carlo Ratti, Ansar Yasar, and David Rickerby. End-user perspective of low-cost sensors for outdoor air pollution monitoring. *Science of the Total Environment*, 607-608:691–705, 2017.
- [2] Balz Maag, Zimu Zhou, and Lothar Thiele. W-Air. *Proceedings of the ACM on Interactive, Mobile, Wearable and Ubiquitous Technologies*, 2(1):1–25, 2018.
- [3] Srinivas Devarakonda, Parveen Sevusu, Hongzhang Liu, Ruilin Liu, Liviu Iftode, and Badri Nath. Real-time air quality monitoring through mobile sensing in metropolitan areas. In *Proceedings of the 2nd ACM SIGKDD International Workshop on Urban Computing*, UrbComp ’13, New York, NY, USA, 2013. Association for Computing Machinery.
- [4] S M Shiva Nagendra, Y Pavan, M V Narayana, Khadirnaikar Seema, and Pooja Rani. Mobile monitoring of air pollution using low cost sensors to visualize spatio-temporal variation of pollutants at urban hotspots. *Sustainable Cities and Society*, 44:520–535, 2019.
- [5] Balz Maag, Zimu Zhou, and Lothar Thiele. A survey on sensor calibration in air pollution monitoring deployments. *IEEE Internet of Things Journal*, 5(6):4857–4870, 2018.
- [6] Mannam Veera Narayana, Devendra Jalihal, and S. M. Shiva Nagendra. Establishing A Sustainable Low-Cost Air Quality Monitoring Setup: A Survey of the State-of-the-Art. *Sensors*, 22(1):1–39, 2022.
- [7] Brandon Feenstra, Vasileios Papapostolou, Sina Hasheminassab, Hang Zhang, Berj Der Boghossian, David Cocker, and Andrea Polidori. Performance evaluation of twelve low-cost pm2.5 sensors at an ambient air monitoring site. *Atmospheric Environment*, 216:116946, 2019.
- [8] A. Aurora. Algorithmic Correction of MOS Gas Sensor for Ambient Temperature and Relative Humidity Fluctuations. *IEEE Sensors Journal*, 22(15):15054–15061, 2022.
- [9] B. Nilson, P. L. Jackson, C. L. Schiller, and M. T. Parsons. Development and evaluation of correction models for a low-cost fine particulate matter monitor. *Atmospheric Measurement Techniques*, 15(11):3315–3328, 2022.
- [10] Olalekan A.M. Popoola, Gregor B. Stewart, Mohammed I. Mead, and Roderic L. Jones. Development of a baseline-temperature correction methodology for electrochemical sensors and its implications for long-term stability. *Atmospheric Environment*, 147:330–343, 2016.

- [11] M. I. Mead, O. A.M. Popoola, G. B. Stewart, P. Landshoff, M. Calleja, M. Hayes, J. J. Baldovi, M. W. McLeod, T. F. Hodgson, J. Dicks, A. Lewis, J. Cohen, R. Baron, J. R. Saffell, and R. L. Jones. The use of electrochemical sensors for monitoring urban air quality in low-cost, high-density networks. *Atmospheric Environment*, 70:186–203, 2013.
- [12] Laurent Spinelle, Michel Gerboles, Maria Gabriella Villani, Manuel Aleixandre, and Fausto Bonavitacola. Field calibration of a cluster of low-cost available sensors for air quality monitoring. Part A: Ozone and nitrogen dioxide. *Sensors and Actuators, B: Chemical*, 215:249–257, 2015.
- [13] Naomi Zimmerman, Albert A. Presto, Srinivasa P.N. Kumar, Jason Gu, Aliaksei Hauryliuk, Ellis S. Robinson, Allen L. Robinson, and R. Subramanian. A machine learning calibration model using random forests to improve sensor performance for lower-cost air quality monitoring. *Atmospheric Measurement Techniques*, 11(1):291–313, 2018.
- [14] Yun Cheng, Xiucheng Li, Zhijun Li, Shouxu Jiang, Yilong Li, Ji Jia, and Xiaofan Jiang. Aircloud: A cloud-based air-quality monitoring system for everyone. In *Proceedings of the 12th ACM Conference on Embedded Network Sensor Systems*, SenSys '14, page 251–265, New York, NY, USA, 2014. Association for Computing Machinery.
- [15] Jacob Devlin, Ming-Wei Chang, Kenton Lee, and Kristina Toutanova. Bert: Pre-training of deep bidirectional transformers for language understanding. *arXiv preprint arXiv:1810.04805*, 2018.
- [16] S. Feinberg, R. Williams, G. S. W. Hagler, J. Rickard, R. Brown, D. Garver, G. Harshfield, P. Stauffer, E. Mattson, R. Judge, and S. Garvey. Long-term evaluation of air sensor technology under ambient conditions in denver, colorado. *Atmospheric Measurement Techniques*, 11(8):4605–4615, 2018.
- [17] Jiayu Li, Simar K. Mattewal, Sameer Patel, and Pratim Biswas. Evaluation of nine low-cost-sensor-based particulate matter monitors. *Aerosol and Air Quality Research*, 20(2):254–270, 2020.
- [18] Kang Ho Ahn, Handol Lee, Hae Dong Lee, and Sang Chul Kim. Extensive evaluation and classification of low-cost dust sensors in laboratory using a newly developed test method. *Indoor Air*, 30(1):137–146, 2020.
- [19] Joel Kuula, Timo Mäkelä, Minna Aurela, Kimmo Teinilä, Samu Varjonen, Óscar González, and Hilikka Timonen. Laboratory evaluation of particle-size selectivity of optical low-cost particulate matter sensors. *Atmospheric Measurement Techniques*, 13(5):2413–2423, 2020.
- [20] Alastair C. Lewis, James D. Lee, Peter M. Edwards, Marvin D. Shaw, Mat J. Evans, Sarah J. Moller, Katie R. Smith, Jack W. Buckley, Matthew Ellis, Stefan R. Gillot, and Andrew White. Evaluating the performance of low cost chemical sensors for air pollution research. *Faraday Discussions*, 189:85–103, 2016.
- [21] Carl Malings, Rebecca Tanzer, Aliaksei Hauryliuk, Provat K. Saha, Allen L. Robinson, Albert A. Presto, and R Subramanian. Fine particle mass monitoring with low-cost sensors: Corrections and long-term performance evaluation. *Aerosol Science and Technology*, 54(2):160–174, 2020.
- [22] K. K. Barkjohn, B. Gantt, and A. L. Clements. Development and application of a united states-wide correction for pm_{2.5} data collected with the purpleair sensor. *Atmospheric Measurement Techniques*, 14(6):4617–4637, 2021.
- [23] A. Aurora. Algorithmic Correction of MOS Gas Sensor for Ambient Temperature and Relative Humidity Fluctuations. *IEEE Sensors Journal*, 22(15):15054–15061, 2022.
- [24] Laurent Spinelle, Michel Gerboles, Maria Gabriella Villani, Manuel Aleixandre, and Fausto Bonavitacola. Calibration of a cluster of low-cost sensors for the measurement of air pollution in ambient air. In *SENSORS, 2014 IEEE*, pages 21–24, 2014.
- [25] David Hasenfratz, Olga Saukh, Silvan Sturzenegger, and Lothar Thiele. IPSN'12 - Proceedings of the 11th International Conference on Information Processing in Sensor Networks. *IPSN'12 - Proceedings of the 11th International Conference on Information Processing in Sensor Networks*, pages 1–5, 2012.
- [26] Olga Saukh, David Hasenfratz, and Lothar Thiele. Reducing multi-hop calibration errors in large-scale mobile sensor networks. In *Proceedings of the 14th International Conference on Information Processing in Sensor Networks*, IPSN '15, page 274–285, New York, NY, USA, 2015. Association for Computing Machinery.
- [27] Chun Lin, Jonathan Gillespie, MD Schuder, W Duberstein, Iain J Beverland, and Mathew R Heal. Evaluation and calibration of aeroqual series 500 portable gas sensors for accurate measurement of ambient ozone and nitrogen dioxide. *Atmospheric Environment*, 100:111–116, 2015.
- [28] Vikas Kumar and Manoranjan Sahu. Evaluation of nine machine learning regression algorithms for calibration of low-cost PM_{2.5} sensor. *Journal of Aerosol Science*, 157:105809, 2021.
- [29] Vera van Zoest, Frank B. Osei, Alfred Stein, and Gerard Hoek. Calibration of low-cost NO₂ sensors in an urban air quality network. *Atmospheric Environment*, 210(2):66–75, 2019.
- [30] Yanwen Wang, Yanjun Du, Jiaonan Wang, and Tiantian Li. Calibration of a low-cost PM_{2.5} monitor using a random forest model. *Environment International*, 133:105161, 2019.
- [31] Pengfei Han, Han Mei, Di Liu, Ning Zeng, Xiao Tang, Yinghong Wang, and Yuepeng Pan. Calibrations of Low-Cost Air Pollution Monitoring Sensors for CO, NO₂, O₃, and SO₂. *Sensors*, 21(1):256, 2021.
- [32] M V Narayana, Devendra Jalihal, and Shiva Nagendra S M. Quantitative analysis for application specific calibration approaches for low-cost sensors for air quality monitoring. *IEEJ Transactions on Electronics, Information and Systems*, 142(10):1166–1171, 2022.

- [33] Marek Badura, Piotr Batog, Anetta Drzeniecka-Osiadacz, and Piotr Modzel. Regression methods in the calibration of low-cost sensors for ambient particulate matter measurements. *SN Applied Sciences*, 1(6):1–11, 2019.
- [34] Kemal Maulana Alhasa, Mohd Shahrul Mohd Nadzir, Popoola Olalekan, Mohd Talib Latif, Yusri Yusup, Mohammad Rashed Iqbal Faruque, Fatimah Ahamad, Haris Hafizal Abd Hamid, Kadaruddin Aiyub, Sawal Hamid Md Ali, Md Firoz Khan, Azizan Abu Samah, Imran Yusuff, Murnira Othman, Tengku Mohd Farid Tengku Hassim, and Nor Eliani Ezani. Calibration model of a low-cost air quality sensor using an adaptive neuro-fuzzy inference system. *Sensors (Switzerland)*, 18(12):4380, 2018.
- [35] Alessandro Bigi, Michael Mueller, Stuart K. Grange, Grazia Ghermandi, and Christoph Hueglin. Performance of NO, NO2 low cost sensors and three calibration approaches within a real world application. *Atmospheric Measurement Techniques*, 11(6):3717–3735, 2018.
- [36] Sachit Mahajan and Prashant Kumar. Evaluation of low-cost sensors for quantitative personal exposure monitoring. *Sustainable Cities and Society*, 57(November 2019):102076, 2020.
- [37] M. Si, Y. Xiong, S. Du, and K. Du. Evaluation and calibration of a low-cost particle sensor in ambient conditions using machine-learning methods. *Atmospheric Measurement Techniques*, 13(4):1693–1707, 2020.
- [38] Said Munir, Martin Mayfield, Daniel Coca, Stephen A. Jubb, and Ogo Osammar. Analysing the performance of low-cost air quality sensors, their drivers, relative benefits and calibration in cities—a case study in Sheffield. *Environmental Monitoring and Assessment*, 191(2), 2019.
- [39] Yuxiang Lin, Wei Dong, and Yuan Chen. Calibrating Low-Cost Sensors by a Two-Phase Learning Approach for Urban Air Quality Measurement. *Proceedings of the ACM on Interactive, Mobile, Wearable and Ubiquitous Technologies*, 2, 2018.
- [40] David H. Hagan, Gabriel Isaacman-Vanwertz, Jonathan P. Franklin, Lisa M.M. Wallace, Benjamin D. Kocar, Colette L. Heald, and Jesse H. Kroll. Calibration and assessment of electrochemical air quality sensors by co-location with regulatory-grade instruments. *Atmospheric Measurement Techniques*, 11(1):315–328, 2018.
- [41] Carl Malings, Rebecca Tanzer, Aliaksei Hauryliuk, Srinivasa P.N. Kumar, Naomi Zimmerman, Levent B. Kara, Albert A. Presto, and R. Subramanian. Development of a general calibration model and long-term performance evaluation of low-cost sensors for air pollutant gas monitoring. *Atmospheric Measurement Techniques*, 12(2):903–920, 2019.
- [42] José María Cordero, Rafael Borge, and Adolfo Narros. Using statistical methods to carry out in field calibrations of low cost air quality sensors. *Sensors and Actuators, B: Chemical*, 267(2):245–254, 2018.
- [43] Pau Ferrer-Cid, Jose M. Barcelo-Ordinas, Jorge Garcia-Vidal, Anna Ripoll, and Mar Viana. Multisensor Data Fusion Calibration in IoT Air Pollution Platforms. *IEEE Internet of Things Journal*, 7(4):3124–3132, 2020.
- [44] Yu Zheng, Furui Liu, and Hsun Ping Hsieh. U-Air: When urban air quality inference meets big data. *Proceedings of the ACM SIGKDD International Conference on Knowledge Discovery and Data Mining*, Part F1288:1436–1444, 2013.
- [45] Huatao Xu, Pengfei Zhou, Rui Tan, Mo Li, and Guobin Shen. LIMU-BERT: Unleashing the Potential of Unlabeled Data for IMU Sensing Applications. *SenSys 2021 - Proceedings of the 2021 19th ACM Conference on Embedded Networked Sensor Systems*, pages 220–233, 2021.
- [46] N. Masson, R. Piedrahita, and M. Hannigan. Approach for quantification of metal oxide type semiconductor gas sensors used for ambient air quality monitoring. *Sensors and Actuators, B: Chemical*, 208:339–345, 2015.
- [47] Xiao Liu, Sitian Cheng, Hong Liu, Sha Hu, Daqiang Zhang, and Huansheng Ning. A survey on gas sensing technology. *Sensors*, 12(7):9635–9665, 2012.
- [48] Balz Maag, Zimu Zhou, and Lothar Thiele. Enhancing multi-hop sensor calibration with uncertainty estimates. In *2019 IEEE SmartWorld, Ubiquitous Intelligence & Computing, Advanced & Trusted Computing, Scalable Computing & Communications, Cloud & Big Data Computing, Internet of People and Smart City Innovation (SmartWorld/SCALCOM/UIC/ATC/CBDCOM/IOP/SCI)*, pages 618–625, 2019.
- [49] Ashish Vaswani, Noam Shazeer, Niki Parmar, Jakob Uszkoreit, Llion Jones, Aidan N. Gomez, Łukasz Kaiser, and Illia Polosukhin. Attention is all you need. In *Proceedings of the 31st International Conference on Neural Information Processing Systems, NIPS’17*, page 6000–6010, Red Hook, NY, USA, 2017. Curran Associates Inc.
- [50] Jimmy Lei Ba, Jamie Ryan Kiros, and Geoffrey E. Hinton. Layer normalization, 2016.
- [51] Dan Hendrycks and Kevin Gimpel. Gaussian error linear units (gelus). *arXiv preprint arXiv:1606.08415*, 2016.
- [52] Junyoung Chung, Caglar Gulcehre, KyungHyun Cho, and Yoshua Bengio. Empirical evaluation of gated recurrent neural networks on sequence modeling. *arXiv preprint arXiv:1412.3555*, 2014.
- [53] US epa data website. <https://catalog.data.gov/dataset/cairsense-denver>. Accessed: 2023-05-14.
- [54] Diederik P Kingma and Jimmy Ba. Adam: A method for stochastic optimization. *arXiv preprint arXiv:1412.3555*, 2014.